Topological Sieving of Rings According to their Rigidity

Stefano Iubini,[*,†] Enzo Orlandini,[†,‡] Davide Michieletto,[¶] and Marco Baiesi[†,‡]

Department of Physics and Astronomy, University of Padova, Via Marzolo 8, I-35131 Padova, Italy , INFN, Sezione di Padova, Via Marzolo 8, I-35131 Padova, Italy , and School of Physics and Astronomy, University of Edinburgh, Peter Guthrie Tait Road, Edinburgh, EH9 3FD, UK

E-mail: stefano.iubini@unipd.it

Abstract

We present a novel mechanism for resolving the mechanical rigidity of nanoscopic circular polymers that flow in a complex environment. The emergence of a regime of negative differential mobility induced by topological interactions between the rings and the substrate is the key mechanism for selective sieving of circular polymers with distinct flexibilities. A simple model accurately describes the sieving process observed in molecular dynamics simulations and yields experimentally verifiable analytical predictions, which can be used as a reference guide for improving filtration procedures of circular filaments. The *topological sieving* mechanism we propose ought to be relevant also in probing the microscopic details of complex substrates.

[*]To whom correspondence should be addressed

[†]Department of Physics and Astronomy, University of Padova, Via Marzolo 8, I-35131 Padova, Italy

[‡]INFN, Sezione di Padova, Via Marzolo 8, I-35131 Padova, Italy

[¶]School of Physics and Astronomy, University of Edinburgh, Peter Guthrie Tait Road, Edinburgh, EH9 3FD, UK

The sieving of fluctuating fibers or polymers according to some of their physical or topological properties is a key process in many research fields ranging from molecular biology[1–3], engineering[4] and polymer physics[5–7]. Beyond its theoretical appeal, the achievement of efficient separation techniques has far reaching industrial[8] and medical[9] applications and potentially broad impact on next-generation polymer-based materials[10]. Most of the sieving techniques exploit the competition between external forcing, surface interactions or entropic trapping of the fibers due to obstacles[7,11]. This gives rise to unique transport properties that mostly depend on either the contour length[12], mass[3] or charge[4] of the filaments. Notably, traditional sieving techniques such as gel electrophoresis can even be employed to detect and separate biopolymers in different topological states[13–15], e.g. linear, circular, knotted or linked, and in turn provide the community with an irreplaceable tool to gain insight into a wide range of problems, from the packaging of DNA bacteriophages[16,17] to the topological action of certain classes of proteins in vivo[18–20]. Automated separation of polymers can also be obtained using microfluidic devices and a recent numerical study has shown that, due to hydrodynamic effects, circular and linear polymers can be separated by a Poiseuille flow within properly decorated micro-channels[21].

Despite the abundance of biologically and medically important circular biomolecules that may differ by their degree of rigidity, e.g., single and double stranded DNA plasmids[12], looped RNA and protein secondary structures[22,23] or intasome-bound viral DNA[24], there is a notable lack of studies aimed at investigating the effect that polymer rigidity may have on the transport properties of circular filaments within either structured fluids such as gels[25] or arrays of obstacles[26,27].

Here we combine nonequilibrium analytical theories and large-scale Brownian dynamics simulations to address this problem by focusing on a model of semiflexible rings forced to move within a mesh of barriers with dangling ends (DE), i.e., fibers that are not part of a closed loop of the gel network[28,29].

We consider semiflexible rings made of beads of diameter σ connected by FENE springs[30]

and interacting via a standard truncated and shifted Lennard-Jones potential. Besides fully rigid circular rings, we explore two values of the chain persistence length $l_p = 20\sigma$ and 5σ, see Supporting Information S1 and Figure S1. The model can then be related to various types of circular biomolecules with different rigidity. Here we focus on rings with contour length $L = 100\sigma$. To fix the ideas, for $\sigma = 2.5$nm, i.e. the typical double-stranded DNA thickness[31], this corresponds to plasmids of about $L = 250\text{nm} \simeq 700$ base pairs.

The structured medium through which the rings migrate is modeled as a sequence of layers with constant gap $l_{\text{gel}} = 80\sigma$ larger than radius of gyration of the rings and orthogonal to the direction x of the force (see Figure S1(b)). Each layer is a static square grid of beads decorated by DE of size $\ell < l_{\text{gel}}$ oriented opposite to the external field. The DE mimic open strands that can be either naturally present in organic gels[32–34] or artificially imprinted in microfluidic arrays[27]. By assuming $\sigma = 2.5$nm, the size of the pores corresponds to $l_{\text{gel}} = 200$nm, comparable to those measured in a 5% agarose gel[25]. Finally, the size of the beads forming the gel is set to $\sigma_g = 10\sigma \simeq 25$nm, close to the average width of both agarose bundles (about 30nm)[25] and nanowires in artificial arrays of obstacles (about 20nm)[27].

To investigate the effect of the substrate geometry, we consider two spatial organizations of the layers: aligned and staggered by $l_{\text{gel}}/2$ in the directions orthogonal to the driving force (see Figure S1(c)). Since the staggered organization displays trapping of rings at lower forces, we choose this arrangement as our default substrate, unless otherwise stated. Each monomer composing the rings is subject to a constant force f in the x direction and its motion through the medium is simulated by evolving the corresponding Langevin equation at fixed volume and constant temperature $T = 1$ (NVT ensemble with Boltzmann constant $k_B = 1$) using a molecular dynamics engine (LAMMPS)[35]. The results are reported as a function of the adimensional force $F = f\sigma/T$, while time is expressed in units of the characteristic time $\tau = 36$ns (see Supporting Information S2 for details).

We first discuss the effect of chain rigidity on the transport properties of the rings. In Figure 1(a,b) we report typical trajectories of the center of mass along the field direction,

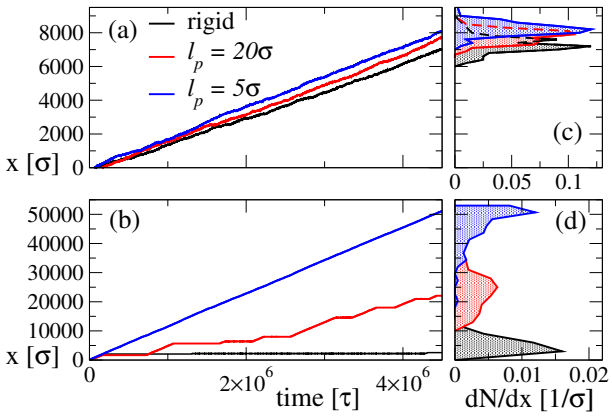

Figure 1: (a,b) Time dependence of the center of mass position of a ring along the force direction for $F = 0.002$ (a) $F = 0.012$ (b). Curves refer to a fully rigid ring (black) and to a ring with persistence length $l_p = 20\sigma$ (red) and $l_p = 5\sigma$ (blue). The DE length is $\ell = 16\sigma$. Panel (c) and (d) are, respectively for case (a) and (b), the resulting late time spatial distributions of a sample of 100 rings.

respectively for $F = 0.002$ and $F = 0.012$, and for $\ell = 2\sigma_g = 16\sigma \simeq 40$nm. In each panel the three curves correspond to different rigidities. In Figure 1(a) the force is very low and no trappings are visible; conversely, in Figure 1(b) trajectories are markedly separated. While most of flexible rings still migrate virtually undisturbed through the medium, those with $l_p = 20\sigma$ display a more complex behavior, alternating runs (velocity $v > 0$) with trappings ($v \simeq 0$). By visual inspection of Brownian dynamics trajectories, we associate trapping events with impalements in which rings are threaded by DE (see also the movie in Supporting Information)[36]. These topologically trapped rings can only re-establish their motion by means of thermal fluctuations that transiently push them against the external field. The strong dependence of trapping and running typical times on rings rigidity gives rise to spatially separated classes of molecules which could be readily detected in electrophoretic experiments (see Figure 1(c,d)). This topological trapping cannot be seen for open filaments[36] but only for looped molecules. In other words, while we expect topologically trivial polymers to display a rigidity-dependent mobility via classic Ogston sieving[11], these should not display trapping-driven topological sieving. Below we argue that this separation pathway may be important for polymers whose size is smaller than the gel pores, as they cannot be clearly

separated via classic sieving[11].

The polymer flow can be quantified by tracking the rings and by measuring their average speed. As shown in Figure (2), all systems display a non-monotonic response with a differential mobility $\mu_{\rm diff} \equiv \frac{\partial \langle v \rangle}{\partial F} < 0$ above a critical force F_c, i.e. a regime of negative differential mobility (NDM). Additionally, the mobility of the rings markedly decreases with ring stiffness at large forces, yet this distinction is weaker or absent for small applied forces. We argue that in the latter regime, rings that become impaled by DE can easily escape by thermal fluctuations; conversely, for very large forces, the escape probability of a trapped ring vanishes. Intriguingly, the most pronounced mobility difference is found at intermediate forces, thus suggesting that this regime may be the best candidate to achieve efficient and fast polymer separation. Finally, in Figure 2(a) we highlight that both the critical force F_c and the response amplitude strongly depend on the ring flexibility; as we discuss below, this novel finding may be employed to refine current gel electrophoresis techniques. As expected, no NDM emerges for linear polymers of the same length, see an example in Figure 2(a).

A minimal two-state model can account for the NDM and provide a simple description of the stationary state[36]. We assume that in the presence of a force F the rings can either be trapped due to topological interactions (impalements) or running. In the running regime, the rings have an average non-zero velocity $v_R = \mu_R F$, where μ_R is the (positive) absolute mobility in the running state. Simulations with no DE ($\ell = 0$) show that μ_R is weakly dependent on F and always lower than the value $\mu_R^{\rm free} = \sigma/\tau$ of a polymer in solvent. Hereafter we use $\mu_R = 0.9\,\sigma/\tau$ as a good approximation of the mobility of non-trapped rings. Given μ_R, the time to drift from one layer to the next is $t_{\rm drift} = l_{\rm gel}/(\mu_R F)$, while the time scale to diffuse over a span $l_{\rm gel}$ is $t_D = l_g^2/(2\mu_R T)$. Diffusion thus is expected to dominate when $t_{\rm drift} > t_D$, i.e. (here using $T = 1$) for $F < \tilde{F} = 2/l_{\rm gel} = 0.025$. Most of our simulations fall in this regime. Hence, the probability per unit time that a ring hits a DE and is impaled, namely the trapping rate $k_{\rm trap}$, is hereafter assumed to be independent on F. We checked that an additional parameter introducing a linear F-dependence of $k_{\rm trap}$

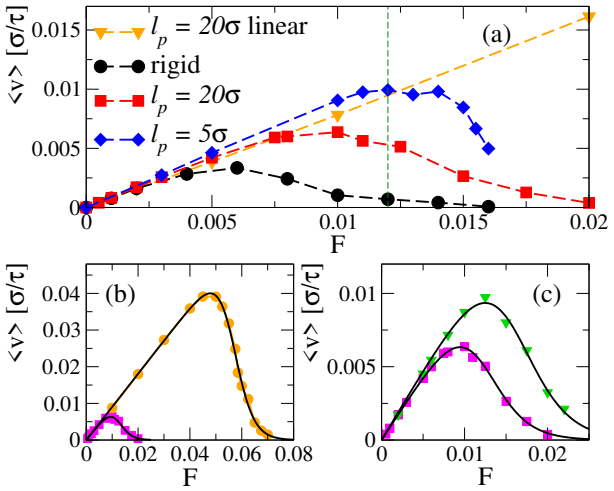

Figure 2: Examples of average ring velocity as a function of the driving F: (a) Data for rings with three rigidities (see legend), with DE length $\ell = 16\sigma$. The vertical line indicates a region with good sieving properties. Dashed lines are guides to the eye. Data for linear polymers with $l_p = 20\sigma$ and contour length $L = 99\sigma$ (orange triangles) show normal mobility, as short open polymers cannot be impaled by DE. In (b) and (c) we compare data for $l_p = 20\sigma$ and $\ell = 16\sigma$ (magenta squares) with runs with (b) shorter DE length $\ell = 8\sigma$ (orange circles) and (c) same parameters but in the cubic version of the gel (green triangles) rather than the staggered layers (default) version. In (b) and (c), continuous curves are fits according to (2).

would not lead to visible improvements.

The transition rate from the trapped to the running state (or escape rate, $k_{\rm esc}$) takes into account an effective local energy barrier $\Delta E/T = \alpha F$ which must be overcome by the ring when leaving the trapped state. By crudely approximating a ring as a point particle driven by F, the energy barrier would assume the simple form $\Delta E/T = F\ell/\sigma$ and the related escape rate $k_{\rm esc}$ would essentially depend on the product $F\ell$ only. However, due to the conformational entropy of the polymers, additional degrees of freedom, such as the ring persistence length l_p, can effectively enter into ΔE and produce more complicated responses. To account for these effects, we write the escape rate in the more general form

$$k_{\rm esc} = \psi \exp(-\alpha F) \tag{1}$$

where the parameters ψ and α may depend on the ring rigidity and on ℓ. By introducing the adimensional parameter $C = k_{\rm trap}/\psi$, we first derive the stationary probability of the

running state $p_R = \exp(-\alpha F)/[C + \exp(-\alpha F)]$. In turn, the average ring velocity reads

$$\langle v \rangle = v_R p_R = \mu_R F \frac{\exp(-\alpha F)}{C + \exp(-\alpha F)} . \tag{2}$$

The curve $\langle v(F) \rangle$ displays a region with NDM. More precisely, one finds $\mu_{\rm diff} < 0$ for $F > F_c$, where F_c solves the equation $C + e^{-\alpha F_c} - \alpha C F_c = 0$. Taking the limit of vanishing trapping, $C \to 0$ (or $\alpha \to 0$), this equation has no physical solution and the function $\langle v(F) \rangle$ becomes linear in F, with a constant positive $\mu_{\rm diff}$. This clarifies that the origin of NDM has to be found in the topological interactions between rings and DE.

In order to compare the analytical predictions with numerical simulations, we probe the nonequilibrium stationary states of the systems. In Figure 2(b) we compare the average velocity obtained from simulations with $l_p = 20\sigma$ and for two DE lengths, and we fit the data with (2). The fits give excellent results (curves in Figure 2(b)) also in the NDM regime. Note that the onset value F_c of NDM drastically increases when ℓ is halved. This behavior is clearly related to the exponential dependence of $k_{\rm esc}$ on the energy barrier $\Delta E \approx \ell$.

Intriguingly, the trapping mechanism is also affected by spatial arrangement of DE in the substrate. As shown in Figure 2(c), systems differing only in the spatial position of the gel layers (aligned or staggered) display distinct responses to F. The staggered substrate reduces more quickly the velocity of the probes by increasing F, as the rings are more easily trapped by its exposed DE. In order words, we discover that $k_{\rm trap}$ can be tuned through the spatial organization of the gel, and it assumes larger values when layers are staggered, although the change in behavior is not as strong as the one consequent to a variation in ℓ.

By tracking single-molecule trajectories, we can also explore the behavior of the trapping and escape rates for different NDM regimes and test whether they follow, respectively, $k_{\rm trap} \simeq$ constant and (1). To this end, we first compute the average velocity $\bar{v}(t)$ of a ring over small temporal windows of 10τ, as shown in inset of Figure 3. This quantity displays reduced fluctuations with respect to the instantaneous ring velocity as well as a clear pattern of

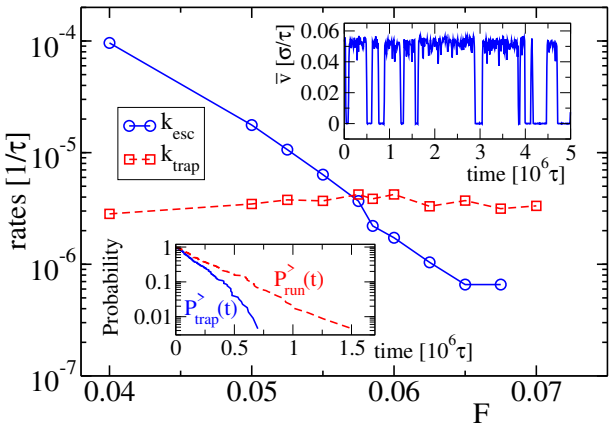

Figure 3: Rates $k_{\rm esc}$ (blue circles) and $k_{\rm trap}$ (red squares) versus force F for an ensemble of rings with $l_p = 20\sigma$ in a gel with $\ell = 8\sigma$. Lines are guides to the eye. Upper inset: typical evolution of the velocity $\bar{v}(t)$ of a ring for $F = 0.055$. Lower inset: integrated probability distributions of trapped and running periods.

alternating running and trapped states, whose typical duration times can then be readily recorded.

Within the two-state model, both the probability distribution $P_{\rm trap}(t)$ of residence times in the trapped state and $P_{\rm run}(t)$ of periods in the running state should follow an exponential decay with time. Hence, their integrated versions are $P^{>}_{\rm trap}(t) \equiv \int_t^\infty P_{\rm trap}(t')dt' = \exp(-k_{\rm esc}\, t)$ and $P^{>}_{\rm run}(t) \equiv \int_t^\infty P_{\rm run}(t')dt' = \exp(-k_{\rm trap}\, t)$, and we can directly calculate the rates $k_{\rm esc}$ and $k_{\rm trap}$ by fitting their exponential scaling (see Figure 3). By repeating the same analysis for systems with different rigidities and DE lengths, we are able to characterize precisely the parameters α, ψ and $k_{\rm trap}$, see Figure 4(a,b,c). In turn, we use the direct evaluation of these parameters from single-molecule trajectories to predict the mobility of the bulk for a given ℓ, l_p and F, with remarkably good results (Figure 4(d)-(f)). The sensitivity of the kinetic parameters to the ring rigidity observed for various ℓ's suggests the robustness of the sieving process also for more realistic environments with heterogeneous dangling ends.

In summary, we have shown that a minimal model for ring polymers traveling through a complex environment with key features of a realistic gel, as the presence of DE, can capture the poorly explained empirical evidence of NDM for circular plasmids[32,34,36,37]. We thus argue that electrostatic interactions, albeit present in real situations, may not be crucial here.

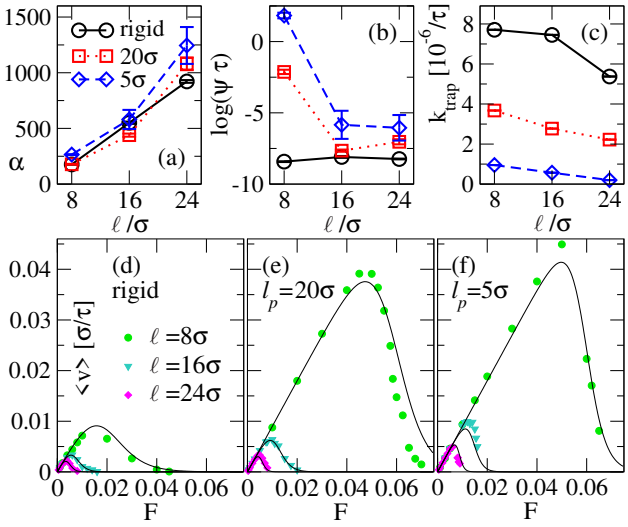

Figure 4: The parameters α (a), ψ (b) and $k_{\rm trap}$ (c) for three plasmid rigidities, plotted vs ℓ. (d) For rigid rings, curves of average plasmid velocity as obtained from numerical simulations for different ℓ's (symbols, see caption) and from the two-states model with parameters shown in (a)-(c) (lines), and (e) the same for semiflexible polymers with $l_p = 20\sigma$ and (f) $l_p = 5\sigma$.

It is important to notice that in this study we have neglected hydrodynamic interactions. These can certainly affect the nonequilibrium dynamics and shape of confined polymers[21,38] but they would not hinder the occurrence of NDM, which is mainly based on the topological interactions between the rings and the dangling ends. Preliminary simulations with hydrodynamic interactions confirm this expectation, see Supporting Information S4.

The onset of NDM may occur at distinct applied forces, depending on the flexibility of the rings, the typical size of dangling ends, and their position. Suitable protocols optimally exploiting NDM can therefore be designed to efficiently separate circular biomolecules with different rigidity, such as RNA and DNA. Importantly, topological sieving can separate molecules that are smaller than the size of the gel pores, a goal impossible to achieve with normal Ogston sieving.

A fascinating consequence of these results is the possibility to use circular polymers drifting through a medium as probes for its microstructure. To this end, a predictive theoretical tool is necessary. Here we have shown that a simple two-state nonequilibrium theory captures remarkably well the sieving process. The trapping and escaping rates can be directly

measured by tracking single molecules drifting through a medium of unknown structure and may be used to directly characterize its complexity.

Acknowledgement

We acknowledge support from Progetto di Ricerca Dipartimentale BIRD173122/17. DM and EO acknowledge networking support by the COST Action CA17139.

Supporting Information Available

Supporting Information

Additional details of the model, simulation setup, physical units, hydrodynamic interactions (pdf). Movie of the system evolution (avi). This material is available free of charge via the Internet at http://pubs.acs.org/.

References

(1) Andrews, P. Estimation of the molecular weights of proteins by Sephadex gel-filtration. *Biochemical Journal* **1964**, *91*, 222.

(2) Porath, J. Sweden: Molecular Sieving and Adsorption. *Nature* **1968**, *218*, 834.

(3) Doenecke, D.; McCarthy, B. J. Protein content of chromatin fractions separated by sucrose gradient centrifugation. *Biochemistry* **1975**, *14*, 1366–1372.

(4) Chung, M.; Kim, D.; Herr, A. E. Polymer sieving matrices in microanalytical electrophoresis. *Analyst* **2014**, *139*, 5635–5654.

(5) Volkmuth, W. D.; Duke, T.; Wu, M. C.; Austin, R. H.; Szabo, A. DNA electrodiffusion in a 2D array of posts. *Phys. Rev. Lett.* **1994**, *72*, 2117–2120.

(6) Alon, U.; Mukamel, D. Gel electrophoresis and diffusion of ring-shaped DNA. *Phys. Rev. E* **1997**, *55*, 1783–1793.

(7) Han, J.; Craighead, H. G. Separation of Long DNA Molecules in a Microfabricated Entropic Trap Array. *Science* **2000**, *288*, 1026–1029.

(8) Corma, A. From Microporous to Mesoporous Molecular Sieve Materials and Their Use in Catalysis. *Chemical Reviews* **1997**, *97*, 2373–2420.

(9) Jee, J.-G.; Kim, M.-B.; Lee, C.-H. Pressure swing adsorption processes to purify oxygen using a carbon molecular sieve. *Chemical Engineering Science* **2005**, *60*, 869–882.

(10) Ligon, S. C.; Liska, R.; Stampfl, J.; Gurr, M.; Mülhaupt, R. Polymers for 3D printing and customized additive manufacturing. *Chemical reviews* **2017**, *117*, 10212–10290.

(11) Viovy, J. Electrophoresis of DNA and other polyelectrolytes: Physical mechanisms. *Rev. Mod. Phys.* **2000**, *72*, 813–872.

(12) Calladine, C. R.; Drew, H.; Luisi, F. B.; Travers, A. A. *Understanding DNA: the molecule and how it works*; Academic Press, San Diego, CA, 2004.

(13) Stasiak, A.; Katritch, V.; Bednar, J.; Michoud, D.; Dubochet, J. Electrophoretic mobility of DNA knots. *Nature* **1996**, *384*, 122.

(14) Weber, C.; Stasiak, A.; De Los Rios, P.; Dietler, G. Numerical simulation of gel electrophoresis of DNA knots in weak and strong electric fields. *Biophys. J.* **2006**, *90*, 3100–3105.

(15) Michieletto, D.; Marenduzzo, D.; Orlandini, E. Topological patterns in two-dimensional gel electrophoresis of DNA knots. *Proc. Natl. Acad. Sci. USA* **2015**, *112*, E5471–E5477.

(16) Trigueros, S.; Arsuaga, J.; Vazquez, M. E.; Sumners, D.; Roca, J. Novel display of knotted DNA molecules by two-dimensional gel electrophoresis. *Nucleic Acids Res.* **2001**, *29*, E67–E67.

(17) Marenduzzo, D.; Orlandini, E.; Stasiak, A.; Sumners, D.; Tubiana, L.; Micheletti, C. DNA-DNA interactions in bacteriophage capsids are responsible for the observed DNA knotting. *Proc. Natl. Acad. Sci. USA* **2009**, *106*, 22269–22274.

(18) Bates, A.; Maxwell, A. *DNA topology*; Oxford University Press, Oxford, U.K., 2005.

(19) Baxter, J.; Sen, N.; Martínez, V. L.; De Carandini, M. E. M.; Schvartzman, J. B.; Diffley, J. F. X.; Aragón, L. Positive Supercoiling of Mitotic DNA Drives Decatenation by Topoisomerase II in Eukaryotes. *Science* **2011**, *331*, 1328–1332.

(20) Cebrián, J.; Kadomatsu-Hermosa, M. J.; Castán, A.; Martínez, V.; Parra, C.; Fernández-Nestosa, M. J.; Schaerer, C.; Martínez-Robles, M.-L.; Hernández, P.; Krimer, D. B.; Stasiak, A.; Schvartzman, J. B. Electrophoretic mobility of supercoiled, catenated and knotted DNA molecules. *Nucleic Acids Res.* **2014**, *3112*, 1–10.

(21) Weiss, L. B.; Nikoubashman, A.; Likos, C. N. Topology-Sensitive Microfluidic Filter for Polymers of Varying Stiffness. *ACS Macro Lett.* **2017**, *6*, 1426–1431.

(22) Micheletti, C.; Di Stefano, M.; Orland, H. Absence of knots in known RNA structures. *Proceedings of the National Academy of Sciences* **2015**, *112*, 2052–2057.

(23) Sułkowska, J. I.; Rawdon, E. J.; Millett, K. C.; Onuchic, J. N.; Stasiak, A. Conservation of complex knotting and slipknotting patterns in proteins. *Proceedings of the National Academy of Sciences* **2012**, *109*, E1715–E1723.

(24) Michieletto, D.; Lusic, M.; Marenduzzo, D.; Orlandini, E. Physical Principles of HIV Integration in the Human Genome. *arXiv:1801.04232* **2018**,

(25) Pernodet, N.; Maaloum, M.; Tinland, B. Pore size of agarose gels by atomic force microscopy. *Electrophoresis* **1997**, *18*, 55–58.

(26) Volkmuth, W. D.; Austin, R. H. DNA electrophoresis in microlithographic arrays. *Nature* **1992**, *358*, 600–602.

(27) Rahong, S.; Yasui, T.; Yanagida, T.; Nagashima, K.; Kanai, M.; Klamchuen, A.; Meng, G.; He, Y.; Zhuge, F.; Kaji, N.; Kawai, T.; Baba, Y. Ultrafast and wide range analysis of DNA molecules using rigid network structure of solid nanowires. *Sci. Rep.* **2014**, *4*, 5252.

(28) Vieira, V. M.; Hay, L. L.; Smith, D. K. Multi-component hybrid hydrogels–understanding the extent of orthogonal assembly and its impact on controlled release. *Chemical science* **2017**, *8*, 6981–6990.

(29) Lee, K. J.; Yun, S. I. Nanocomposite hydrogels based on agarose and diphenylalanine. *Polymer* **2018**, *139*, 86–97.

(30) Klenin, K.; Langowski, J. Computation of writhe in modeling of supercoiled DNA. *Biopolymers* **2000**, *54*, 307–317.

(31) Rybenkov, V. V.; Cozzarelli, N. R.; Vologodskii, A. V. Probability of DNA knotting and the effective diameter of the DNA double helix. *Proc. Natl. Acad. Sci. USA* **1993**, *90*, 5307–5311.

(32) Mickel, S.; Arena, V.; Bauer, W. Physical properties and gel electrophoresis behavior of R12-derived plasmid DNAs. *Nucleic Acids Res.* **1977**, *4*, 1465–1482.

(33) Levene, S. D.; Zimm, B. H. Separations of open-circular DNA using pulsed-field electrophoresis. *Proc. Natl. Acad. Sci. USA* **1987**, *84*, 4054–4057.

(34) Åkerman, B.; Cole, K. Electrophoretic capture of circular DNA in gels. *Electrophoresis* **2002**, *23*, 2549–2561.

(35) Plimpton, S. Fast Parallel Algorithms for Short-Range Molecular Dynamics. *J. Comp. Phys.* **1995**, *117*, 1–19.

(36) Michieletto, D.; Baiesi, M.; Orlandini, E.; Turner, M. S. Rings in random environments: sensing disorder through topology. *Soft Matter* **2014**, *11*, 1100–1106.

(37) Akerman, B. Effects of supercoiling in electrophoretic trapping of circular DNA in polyacrylamide gels. *Biophys. J.* **1998**, *74*, 3140–3151.

(38) Hsiao, K.-W.; Schroeder, C. M.; Sing, C. E. Ring Polymer Dynamics Are Governed by a Coupling between Architecture and Hydrodynamic Interactions. *Macromol.* **2016**, *49*, 1961–1971.

Graphical TOC Entry

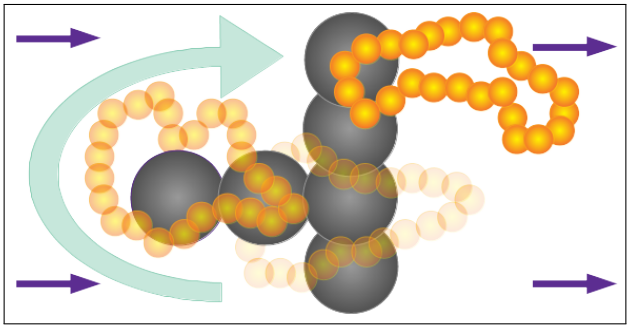

Supporting Information for "Topological Sieving of Rings According to their Rigidity"

Stefano Iubini,*,† Enzo Orlandini,† Davide Michieletto,¶ and Marco Baiesi†

Department of Physics and Astronomy, University of Padova, Via Marzolo 8, I-35131 Padova, Italy , INFN, Sezione di Padova, Via Marzolo 8, I-35131 Padova, Italy , and School of Physics and Astronomy, University of Edinburgh, Peter Guthrie Tait Road, Edinburgh, EH9 3FD, UK

E-mail: stefano.iubini@unipd.it

S1 Model and numerical procedure

Rings are modeled as closed polymer chains each made of $M = 100$ beads of diameter $\sigma = 2.5\,nm$ that move in a static cubic gel with total linear dimension $640\sigma = 8l_g$ and periodic boundary conditions in all three directions. Figure S1 shows a typical configuration of the whole system (panel (a)) and the details of the gel structure (panels b and c).

In the following, we denote by $\vec{r}_i$ the position of the i-th bead and by $d_{i,j} = |\vec{d}_{i,j}| = |\vec{r}_i - \vec{r}_j|$ the distance between two beads. The steric interaction between beads belonging to polymer rings and the interaction between a polymer bead and a gel bead is modeled by a truncated

*To whom correspondence should be addressed
†Department of Physics and Astronomy, University of Padova, Via Marzolo 8, I-35131 Padova, Italy
‡INFN, Sezione di Padova, Via Marzolo 8, I-35131 Padova, Italy
¶School of Physics and Astronomy, University of Edinburgh, Peter Guthrie Tait Road, Edinburgh, EH9 3FD, UK

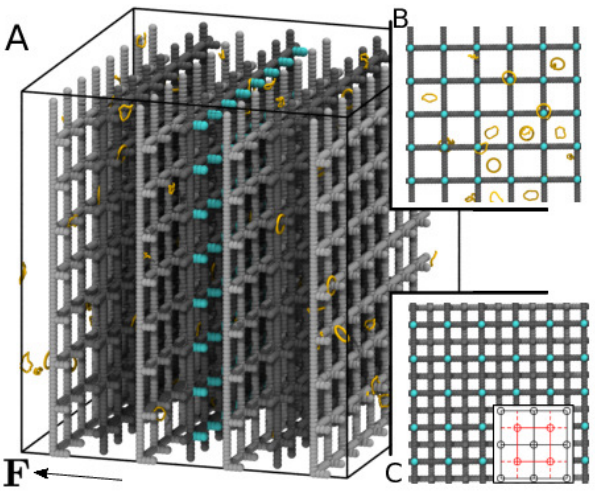

Figure S1: (a) Snapshot of a part of the gel structure, made of stacked and staggered square grids (alternated dark and light gray) displaying dangling ends (DE, some highlighted in cyan) of length $\ell = 24\sigma$, the longest used in this work. Ring polymers (yellow) of three kinds (fully rigid circles, $l_p = 20\sigma$ and $l_p = 5\sigma$) are forced through the gel and their position tracked in time. (b) Zoom in the gel showing only one layer of the gel structure where some of the rings are trapped by the DE. (c) Zoom in the gel highlighting the staggered arrangement of two consecutive grids.

and shifted Lennard-Jones potential

$$U_{LJ}(i,j) = 4\epsilon \left[\left(\frac{\sigma_c}{d_{i,j}} \right)^{12} - \left(\frac{\sigma_c}{d_{i,j}} \right)^{6} - \frac{1}{4} \right] \Theta\left(2^{\frac{1}{6}} \sigma_c - d_{i,j} \right) \quad , \tag{S1}$$

where ϵ is the typical energy scale of the interaction potential and $\Theta(x)$ is the Heaviside function. The parameter σ_c plays the role of a minimum distance between beads and depends on the bead type. If i and j are both polymer indexes, we set $\sigma_c = \sigma$, otherwise, for the interaction between a polymer bead and a gel bead, we define $\sigma_c = (\sigma + \sigma_g)/2 = 5.5\sigma$. The beads forming the polymer mesh do not evolve in time and they are excluded from the computation of mutual interaction terms. The connectivity of each polymer chain is reinforced by a Finitely Extensible Nonlinear Elastic (FENE) potential acting between two consecutive polymer beads i and $i+1$

$$U_{\text{FENE}}(i,i+1) = -\frac{A_F}{2} R_0^2 \log \left[1 - \left(\frac{d_{i,i+1}}{R_0} \right)^2 \right] \tag{S2}$$

for $d_{i,i+1} < R_0$ and $U_{\rm FENE} = +\infty$ otherwise. Here we choose $A_F = 30\epsilon/\sigma^2$ and $R_0 = 1.6\sigma$. Finally, the bending rigidity of the polymer rings is described by a Kratky-Porod potential

$$U_b(i-1,i,i+1) = \frac{k_B T\, l_p}{2\sigma}\left[1 - \frac{\vec{d}_{i-1,i}\cdot\vec{d}_{i,i+1}}{d_{i-1,i}d_{i,i+1}}\right] \tag{S3}$$

where the persistence length l_p is set to 20σ or 5σ for the two finitely flexible classes of rings considered in this Letter. Rigid rings would correspond to $l_p \to \infty$ and they are modeled by adding explicitly a rigidity constraint to their bead configurations. This implies that only Lennard-Jones potential terms are considered for the dynamics of rigid rings.

Introducing the total potential energy $U = U_{LJ} + U_{\rm FENE} + U_b$, the dynamics of the ring beads is described within a Langevin equation

$$m\frac{d^2\,\vec{r}_i}{dt^2} = -\vec{\nabla}U + f\hat{x} - \gamma\frac{d\,\vec{r}_i}{dt} + \vec{\xi}_i(t) \tag{S4}$$

where m is the mass of one polymer bead, γ is a (constant) friction coefficient and $f\hat{x}$ is the external constant force oriented along the positive x direction. The last term $\vec{\xi}_i(t)$ is a Gaussian noise with zero mean and delta-correlated in time. Denoting by $\xi_i^{(\alpha)}$ with $\alpha = 1,2,3$ the Cartesian component of $\vec{\xi}_i$ in the α direction, the noise satisfies a standard fluctuation-dissipation relation in the form

$$\left\langle \xi_i^{(\alpha)}(t)\xi_j^{(\beta)}(t')\right\rangle = 2\gamma k_B T\delta_{i,j}\delta_{\alpha,\beta}\delta(t-t') \tag{S5}$$

The system is evolved starting from an initial condition composed by M planar circular rings randomly placed in the gel structure. Their position and orientation are chosen in order to avoid any initial impalement by a gel dangling end or any irreversible link with the gel structure. The system is first thermalized for a time t_0 at temperature T with $f = 0$ (no external driving) and later evolved for a time t_f in the presence of the external force. Averages are performed at least over 20 trajectories of different rings within the same system,

in a diluted phase in which they do not interact significantly with each other. Simulations are long enough to allow the rings to explore the trapped and running states on timescales much shorter than the total observation time.

S2 Parameters and physical units

In our simulations, the system temperature T is measured in units of ϵ/k_B, with $k_B = \epsilon = 1$. We set the monomer mass $m = 1$ and we measure distances in units of σ. With this choice, the characteristic time scale of the system $\tau = \sigma\sqrt{m\epsilon}$ is unitary. As customary[S1] , we set $m/\gamma = \tau$. In order to estimate the time τ in physical units, we proceed as follows. From the Stokes formula of the friction coefficient for spherical beads with radius $\sigma/2$, we have $\gamma = 3\pi\eta_{sol}\sigma$, where η_{sol} is the viscosity of the solvent. By using the nominal water viscosity at room temperature, $\eta_{sol} = 1cP$, and setting $T = 300K$ and $\sigma = 2.5\,nm$, we get $\tau = 3\pi\eta_{sol}\sigma^3/(k_BT) = 36\,ns$.

The numerical integration of Eq.(S4) is performed by employing a Verlet algorithm with time step $\delta t = 0.01\tau \simeq 0.4\,ns$. For our simulations we choose the thermalization time $t_0 = 2 \times 10^5\tau \simeq 7\,ms$, while the time t_f ranges from a minimum of $5 \times 10^6\tau \simeq 0.18\,s$ to a maximum of $2 \times 10^7\tau \simeq 0.72\,s$ depending on the typical time necessary to reach the nonequilibrium stationary state.

We conclude this section by observing that from the relation $F = f\sigma/(k_BT)$, the force acting on a single polymer bead amounts to $f = 1.7F\,pN$. Since the size of each monomer is $\sigma = 2.5\,nm = 7\,pb$ and each base pair contains two phosphate groups, we approximate the charge of each bead to $Q = 14e$, where e is the electron charge. Hence, we find for characteristic strength of the dragging electric field $E = f/Q \simeq 8 \times 10^3 F\,Vcm^{-1}$. Our results show that topological sieving typically occurs in the interval from $F \simeq 10^{-3}$ to $F \simeq 10^{-2}$, i.e. between $8\,Vcm^{-1}$ and $80\,Vcm^{-1}$.

S3 Movie of the system evolution

The video file named `movie_fig2.avi` shows the evolution of an ensemble of 20 polymer rings flowing in the gel structure. The video shows the trajectory corresponding to the red curve of Figure 1b ($F = 0.012$, $l_p = 20\sigma$). The evolution is shown from $t = 1.1 \times 10^6\,\tau$ to $1.4 \times 10^6\,\tau$.

S4 Hydrodynamic interactions

We have performed preliminary simulations in which hydrodynamic modes are introduced with the Stochastic Rotation Dynamics (SRD) method[S2,S3] .

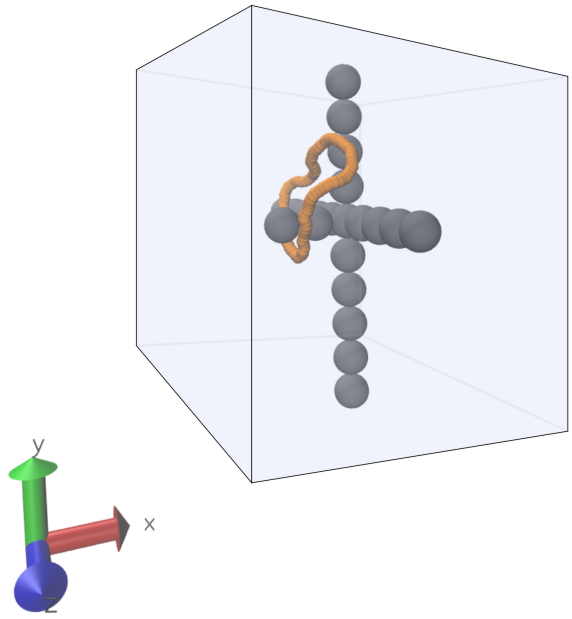

Figure S2: The SRD setup: a polymer ring moves through a gel structure composed of one dangling end in the presence of explicit solvent.

Figure S2 shows the simulation setup and a snapshot of the system dynamics. We consider a minimalist cubic gel structure (grey beads) with one dangling end with $\ell = 16\sigma$ and one polymer ring (small orange beads) with persistence length $l_p = 20\sigma$ and $L = 100\sigma$. The system is contained in a box with linear length $L = 80\sigma$ with periodic boundary conditions.

Explicit solvent and SRD dynamics are included according to the parametrization in[S4] . In particular, we set the number of solvent particles (not shown in Figure S2) equal to 10^6 , which produces a ring mobility $\mu = \langle v \rangle / F$ order 1 (in model units) in the running state. This mobility regime is comparable with the case of implicit Langevin simulations, where $\mu = 1$. Solvent particles interact both with the gel and with the polymer ring.

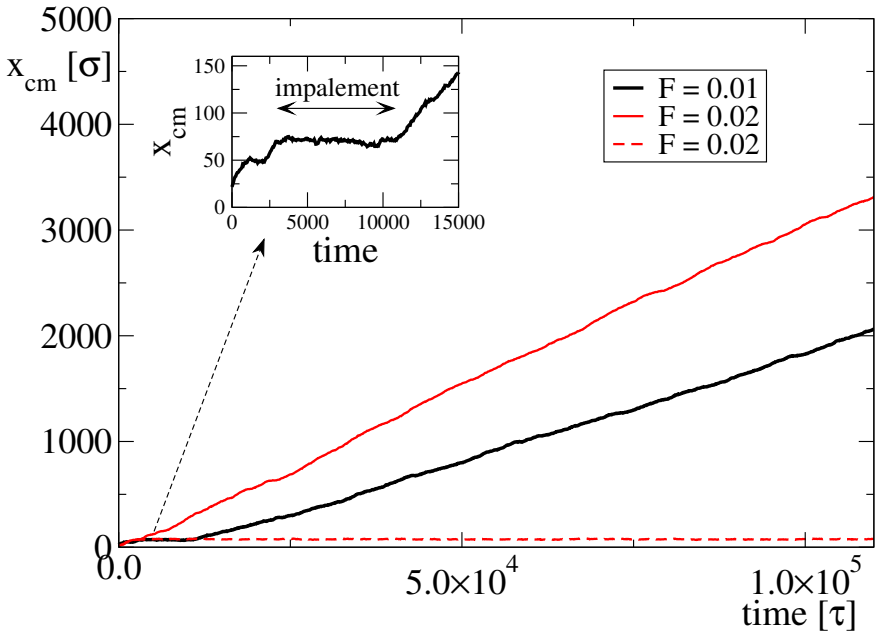

Figure S3: Center of mass position of the ring as a function of time for two values of external force F with explicit SRD solvent.

Figure S3 shows some ring trajectories (center of mass position along the force direction x vs time) in which impalement events are visible (flat parts) for two values of force F. The two red (solid and dashed) curves refer to two independent realizations of the SRD for $F = 0.02$. Consistently with the Langevin description, we observe a dramatic increase of the impalement time (see black and red dashed curves) upon increasing the force. This supports the existence of ring negative differential mobility even in the presence of hydrodynamic interactions. The relatively short number of impalement events should not surprise on the time scales reached in these preliminary simulations (order $10^5\,\tau$). Indeed, from the analysis reported in Figure 4(c), the typical trapping rate is order $10^{-6}\,\tau^{-1}$. Therefore, much longer trajectories would be needed to perform a statistical analysis of trapping and escape events.

We leave this numerically challenging task to future work.

References

[S1] Kremer, K.; Grest, G. S. Dynamics of entangled linear polymer melts: A molecular-dynamics simulation. *J. Chem. Phys.* **1990**, *92*, 5057.

[S2] Malevanets, A.; Kapral, R. Mesoscopic model for solvent dynamics. *J. Chem. Phys.* **1999**, *110*, 8605–8613.

[S3] Ihle, T.; Kroll, D. Stochastic rotation dynamics: A Galilean-invariant mesoscopic model for fluid flow. *Physical Review E* **2001**, *63*, 020201.

[S4] Weiss, L. B.; Nikoubashman, A.; Likos, C. N. Topology-Sensitive Microfluidic Filter for Polymers of Varying Stiffness. *ACS Macro Lett.* **2017**, *6*, 1426–1431.